Tuning selectivity of acidic carbon dioxide electrolysis via surface modification

Elli Vichou, Alessandro Perazio, Yanis Adjez, Maria Gomez-Mingot, Moritz W. Schreiber, Carlos M Sánchez-Sánchez, Marc Fontecave

Tuning selectivity of acidic carbon dioxide electrolysis via surface modification

Elli Vichou[1], Alessandro Perazio[1], Yanis Adjez[2], Maria Gomez-Mingot[1]*, Moritz Schreiber[3], Carlos M. Sánchez-Sánchez[2]*, Marc Fontecave[1]*

AFFILIATIONS

[1] Laboratoire de Chimie des Processus Biologiques, CNRS UMR 8229, Collège de France, Sorbonne Université, 75005, Paris, France

[2] Laboratoire Interfaces et Systèmes Electrochimiques (LISE), CNRS UMR 8235, Sorbonne Université, 75005, Paris, France

[3] Total Research and Technology, Refining and Chemicals, Division CO_2 Conversion, Feluy, 7181, Seneffe, Belgium

*Corresponding authors. Email: marc.fontecave@college-de-france.fr; carlos.sanchez@sorbonne-universite.fr; maria.gomez@college-de-france.fr

ABSTRACT

Electrocatalytic CO_2 reduction to energy-dense organic compounds useful for the industry is an interesting strategy for organic synthesis using non-fossil carbon feedstocks and for storing energy from intermittent sources in the form of chemical energy. Electrolysis under acidic conditions has been recently studied as a promising way to avoid carbon loss, due to the inevitable carbonate formation using traditional neutral or alkaline electrolytes. Here we report one of the very first examples showing that a molecular modification of the surface of copper nanoparticles allows tuning the selectivity of the reaction towards favoring C_2 products, ethylene and ethanol, at industrially relevant current densities at acidic pH (<1). This is achieved thanks to the electrodeposition of an imidazolium-based layer on the nanoparticles and performing electrolysis using a gas-fed flow cell with an acidic catholyte. Moreover, acidic CO_2 electroconversion in the absence of alkali cations is reported for the first time, providing new perspectives as for addressing the problems associated with the utilization of catholytes containing alkali cations.

INTRODUCTION

CO_2 electroreduction (CO_2RR) has become an important research direction as a way to store intermittent sources of electricity and to valorize CO_2 as a carbon feedstock, instead of fossil carbon, towards chemicals useful for the chemical industry, such as carbon monoxide, hydrocarbons and alcohols[1–3]. Among those products, the C_2 products, ethylene and ethanol in particular, have been considered as a priority target considering the size of the market[4–7]. While still not mature enough for industrial implementation, a number of challenges have already been successfully addressed. First, conversion of CO_2 to ethylene/ethanol can be achieved with relatively high selectivity thanks to Cu-based catalysts, Cu being the unique metal allowing C-C coupling[8–10]. Second, mass transport limitations associated with the low solubility of CO_2 in water have been addressed by shifting from liquid phase electrolyzers (H-cells) to gas phase electrolyzers (flow cells using gas diffusion electrodes-GDE)[11,12]. The latter allow the utilization of alkaline KOH electrolytes which favor high current densities (hundreds of $mA.cm^{-2}$) and C-C coupling reactions. However it was soon realized that the now common use of alkaline or neutral electrolyte solutions limits conversion yields and carbon utilization due to the reaction of CO_2 with hydroxide ions leading to the formation of (bi)carbonate [13,14]. The resulting degradation of the electrolyte and the energetic and economical cost associated with its regeneration have raised some doubts regarding the future potential of alkaline flow-cells[13,14]. The problem can be partly addressed by using acidic electrolyte solutions where the pH is below the pKa of aqueous CO_2. In such systems, while the CO_2 is still converted to (bi)carbonate at high current densities by the alkaline local pH at the cathode arising from hydroxide ions generated during CO_2 reduction, CO_2 is subsequently regenerated due to the low bulk pH[15–18].

Obviously, a major drawback of acidic electrolysis is the propensity for hydrogen production (HER) due to the high concentration of protons. One strategy for limiting HER and promoting CO_2RR is the addition of alkali metal cations M^+. It has been indeed clearly established that M^+ ions within the electrolyte are essential for CO_2RR under acidic conditions likely because accumulation of such partially dehydrated cations on the surface of the cathode can stabilize CO_2-derived adsorbed intermediates and inhibit proton migration thus limiting the rate of HER[18,19]. However high concentrations of M^+ can be detrimental as they promote bicarbonate precipitation on the GDE due to the high local pH and low solubility of $MHCO_3$, thus blocking CO_2 transport. Furthermore, M^+ at high concentration accumulates within the cation-exchange membranes (Nafion) thus adding extra ohmic losses and accelerating their degradation, so that the nature and the concentration of M^+ have to be carefully tuned[20]. For that reason, there is a need to develop strategies for avoiding the utilization of M^+-based electrolytes.

Another strategy for controlling the activity and selectivity of solid electrocatalysts for CO_2RR lies on molecular modification of the electrode surface, using small molecules or polymers[21–25]. This strategy, while extensively used in H-cells and flow cells working in neutral pH and alkaline electrolytes, respectively, has not been explored yet in the context of acidic electrolysis under industrially relevant current densities. Here we show that modification of the surface of Cu nanoparticles (CuNPs) by immobilization of an ionic liquid (IL) based on an imidazolium salt results in the promotion of C_{2+} products when CO_2RR is carried out in flow cells using a highly acidic electrolyte (pH ≤ 1). During the course of this work another study reported promotion of C_{2+} product formation by deposition of a molecular film derived from a pyridinium salt on Cu under acidic conditions (pH = 2)[26].

The choice of an imidazolium salt, as a proof of concept regarding the impact of Cu surface modification on CO_2RR selectivity during acidic electrolysis, was based on previous results, including some from our laboratory[27–30]. The very first studies were carried out with Ag[31–35] and Au[36,37] catalysts, showing a positive impact of the addition of IL (either in solution or dropcast on the electrode surface) on overpotentials and on the selectivity (CO_2RR to CO vs. HER). However, the mechanistic basis for this effect has remained controversial and several hypotheses have been indeed proposed: suppression of HER; accumulation of CO_2 at the surface; formation of adducts between IL and CO_2; stabilization of high-energy CO_2-derived intermediates. Cu-based electrodes functionalized with ILs have been studied much more recently. So far it was limited to H-cells using CO_2-saturated $KHCO_3$ solutions, thus providing low current densities (< 30 $mA.cm^{-2}$),[38,39] and flow cells for alkaline electrolysis using poly-ionic liquids (PILs)[40,41]. In all these cases, IL promoted C_{2+} product formation, and ethylene more specifically. In the present study, we report the first results evaluating a Cu-IL electrode for CO_2RR under highly acidic conditions (pH ≤ 1), at industrially relevant current densities, not only in the presence but also in the absence of alkali metal cations in the electrolyte.

EXPERIMENTAL SECTION

Materials: Cu nanopowder of 60-80 nm size (Sigma-Aldrich, ≥ 99.5 %) was used to prepare the cathodes, except in the case of solvothermal CuO nanoparticles (STCu200), which were synthesized from Cu (II) acetate (Sigma-Aldrich, 99.99 %). For the cathode preparation were also used hydrophobic polytetrafluoroethylene (PTFE) membrane filters (Sartorius, 0.45 µm pore size), methanol (Carlo Erba, 99.9 %) and Nafion 117 (Sigma-Aldrich, 5 wt % in lower aliphatic alcohols and water). As anodes were used Nickel foam and Nickel coil disks (Goodfellow) and the separation was ensured by a bipolar membrane

(Fumasep). The electrolytes were prepared using Milli-Q H_2O, KCl (Sigma Aldrich, ≥ 99 %), KOH (Sigma-Aldrich, 90 %) and H_2SO_4 (Sigma-Aldrich, 95-98 %). The IL electrodeposition was performed using 1-ethyl-3-methylimidazolium tetrafluoroborate ($EMIMBF_4$) (Iolitec, > 98 %, 33.8 cP). For NMR analysis Terephthalic acid (Sigma-Aldrich, 98 %) and D_2O (Eurisotop, 99.9% D) were used.

STCu200 Nanoparticle synthesis: Firstly, 0.74 g of Cu (II) acetate were dissolved in 80 mL of ethanol (Sigma-Aldrich, 96 %) and sonicated for 2-3 h. The resulting completely dissolved solution was blue in color and was placed initially in the PTFE liner of an autoclave (125 mL, Parr Instrument Company) before being transferred to an oven, in which it was heated at 200 °C for 20 h [42]. Subsequently, the solution obtained was clear and the CuO nanoparticles, which were of a dark brown color, had remained deposited at the bottom of the liner. Finally, the nanoparticles underwent several washings, twice with distilled water, then thrice with ethanol and were placed to dry under vacuum for at least 24 h before use. The size of the STCu200 CuNPs was approximately 50 nm and their yield was approximatively 80 %.

PTFE-based GDE Preparation: The cathodes used were gas diffusion electrodes (GDEs) prepared by spraying a methanolic solution containing the Cu nanoparticles (Cu NPs) (10 $mg.mL^{-1}$) on PTFE using Nafion as a binder (1 to 1 ratio of Cu NPs(mg) to Nafion(µL)). The suspension was first sonicated for 10 minutes to ensure that the particles were well dispersed. The ink was then deposited by spraying onto a PTFE membrane using a spray gun (Model Airbrush 180). The sprayed surface was confined to a circular diameter of 2 cm^2, which led to a total mass loading of approximately 2.25 $mg.cm^{-2}$ of each cathode after drying under vacuum in a desiccator. All GDEs require an activation protocol prior to use to reduce all Cu to Cu^0. This activation involved consecutive linear sweep voltammograms (LSVs) under CO_2 flow in a 3 M KCl (pH = 6.2) electrolyte with a sweep rate of 25 $mV.s^{-1}$ varying between −0.5 and −1.9 V vs. Ag/AgCl until stabilization of the current response (Figure S1).

IL Electrodeposition: The optimal IL deposition is performed by applying -10 $mA.cm^{-2}$ for 30 minutes on the Cu GDEs in a 0.5 M $EMIMBF_4$ aqueous solution under inert atmosphere and then allowing the electrode to reach open circuit potential. The electrodeposition can take place in a separate container or within the flow cell at a flow rate of 9 $mL.min^{-1}$ by replacing the catholyte container with one containing the 0.5 M $EMIMBF_4$ aqueous solution. When the deposition takes place in a separate container, the electrode is subsequently removed from this deposition solution, rinsed thoroughly with water, and placed in the flow cell to perform CO_2RR experiments. Alternatively, it can take place within the flow cell, in which case water should be subsequently flowed for at least 2 minutes as catholyte to ensure excess IL is removed from the configuration before replacing the catholyte and running CO_2RR experiments.

Electrochemical Experiments: All electrochemical experiments were conducted using either a VSP300 or a VMP3 potentiostat (BioLogic Instruments) with a 20 A current booster and were carried out in the same custom-made gas-fed flow cell purchased from Sphere Ltd[24]. A Ni-foam was used as anode and a leak-free $Ag/AgCl/KCl_{3.4M}$ reference electrode (Innovative Instruments Ltd.) was inserted in the cathodic compartment, while a bipolar membrane in reverse bias mode (Fumasep, stored in 1 M KCl) ensured separation of the two compartments. The conductivity of the PTFE-based GDEs was ensured by Cu tape and their geometric surface area was confined to 1 cm^2. The CO_2 inlet flow rate was kept stable at 10 $mL.min^{-1}$ using a mass flow controller (Bronkhurst), the values were verified using a gas flow meter (MesaLabs Defender 530+) and the data were obtained using the flow meter data logging software (MesaLabs DryCalPro). The acidic catholyte composition was either 0.05 M H_2SO_4 + 3 M KCl (pH = 0.89) or 0.1 M H_2SO_4 (pH = 0.7) and the anolyte was a 2.5 M KOH solution (pH = 14) and both were circulated using a peristaltic pump at a rate of 9 $mL.min^{-1}$. The catholyte was also under constant purging with Argon at a fixed flow rate of 35 $mL.min^{-1}$.The outlet of the catholyte reservoir was then connected to a gas trap, which in turn was connected to the GC, in order to carry the gas products saturated with electrolyte to the on-line GC. The catholyte and anolyte volumes were 25 mL each and the electrolysis time was fixed at 30 min for all experiments except for the 5 h electrolysis stability experiments, where the volumes were increased to 50 mL. The pH of both catholyte and anolyte was monitored after electrolysis and the changes were small ($\Delta pH < 1$). In controlled current electrolysis experiments, the gas products were recorded at 20 min, while the liquid products were sampled after the end of the electrolysis, at 30 min. For the 5 h experiment, liquid samples were extracted using a syringe every hour and the gas products recorded every 20 min.

Analysis of Gas Products: All gas products were detected and quantified in an on-line GC configuration. The GC was purchased from SRI instruments (8610 GC) and Argon was used as the carrier gas. The GC was fitted with both a flame-ionization detector (FID) coupled to a methanizer to allow detection of carbon products (CO, C_2H_4, CH_4) and a thermal conductivity detector (TCD) for H_2 quantification. Before reaching the detectors, the gas was separated using a HaySepD precolumn with a 3 m molecular sieve column. The GC was periodically calibrated using a custom-made standard gas mixture containing all possible products in CO_2.

The Faradaic Efficiency (FE) for gas products was calculated according to the following equation:

$$FE\ (\%) = \frac{n_{product} \times n_{electrons} \times F}{(Q_{t=0} - Q_{t=x})}$$

Where $n_{product}$ is the mol amount of product obtained from electrolysis, $n_{electrons}$ is the number of electrons consumed to produce it, F is the Faraday constant ($C.mol^{-1}$), $Q_{t=0}$ is the charge in Coulomb at the instant of injection, and $Q_{t=x}$ is the charge in Coulomb at time x seconds prior to the injection, x-0 represents the time necessary to fill the sample loop and x depends on both the loop size and total combined flow rate of Ar and CO_2 used[24].

Analysis of Liquid Products: Liquid products were analyzed using ^1H NMR performed on a Bruker Advance III 300 MHz NMR spectrometer (300 K). For sample preparation, an NMR tube was filled with the lock solvent (D_2O, 100 µL), an aqueous solution of the internal standard used for quantification (5 % terephthalic acid (TPA) solution, 100 µL), basic solution to ensure TPA was soluble (5 M KOH, 400 µL) and the electrolysis sample containing products to be quantified (400 µL). Liquid sampling from the anolyte was also performed to ensure that any product crossover through the bipolar membrane was also accounted for.

Physical Characterization: Scanning Electron Microscopy (SEM), Energy-Dispersive X-ray Spectroscopy (EDX) analysis and EDX elemental mapping were all performed using an Ultra 55 ZEISS microscope equipped with a spectrometer Quantax purchased from Bruker and the binding energy was calibrated using a Cu disk. Prior to all analyses the GDEs had been washed with MiliQ H_2O, dried overnight in a desiccator and a coating of carbon was applied to them to ensure conductivity. X-Ray Photoelectron Spectroscopy (XPS) spectra were also acquired on the PTFE GDEs, using an Omicron Argus X-ray photoelectron spectrometer, which was equipped with a monochromated AlKα radiation source (hν = 1486.6 eV), as well as a 280 W electron beam power. The diameter of analyzed area on the PTFE GDEs was 1 mm^2. The emission of photoelectrons from the GDEs was analyzed at a takeoff angle of 45° under ultra-high vacuum conditions (≤ 10−9 mbar). Survey spectra were also carried out with a 100 eV pass energy and for the high-resolution N 1s spectra the pass energy was 20 eV. All binding energies were calibrated against the C 1s (C-C) binding energy at 284.8 eV and Scofield factors were used to correct the elements' peak intensities. The spectra were fitted using Casa XPS v.2.3.15 software (Casa Software Ltd, U.K.) and applying a Gaussian:Lorentzian ratio (G:L) equal to 70:30. Attenuated total reflection Fourier transform infrared spectroscopy (ATR-FTIR) measurements were obtained using a Brucker VERTEX 70 FTIR spectrometer equipped with a diamond ATR accessory (Quest™, Specac). The spectra were collected in the wavenumber range from 400 cm^{-1} to 4000 cm^{-1}, maintaining a spectral resolution of 4 cm^{-1}. Each spectrum was obtained from an aggregate of 100 scans to enhance the signal-to-noise ratio. Post acquisition, the spectra were processed through a series of steps including baseline correction,

atmospheric vapor compensation (water vapor and CO_2 signal subtraction) and a smoothing function for improved clarity and precision in spectral features. Water contact angle (WCA) was measured using a Drop Shape Analyzer (DSA25) from KRÜSS. The measurements were performed at room temperature and ambient humidity on the CuNP GDE samples. Each sample was measured at three different locations and the average value was reported.

ECSA measurements: The electrochemical surface area (ECSA) was measured through the capacitance of the PTFE GDEs in 0.05 M H_2SO_4 + 3 M KCl solution saturated with Argon and CO_2. The capacitance was measured by analyzing the cyclic voltammograms of the cathodes at -0.495 V vs. Ag/AgCl using the following equation:

$$C.\upsilon = \frac{j_a - j_c}{2}$$

where C is the capacitance (F), j_a is the anodic current density at -0.495 V vs. Ag/AgCl ($A.cm^{-2}$), j_c is the cathodic current density at -0.495 V vs. Ag/AgCl ($A.cm^{-2}$) and υ is the scan rate ($V.s^{-1}$). The value of the capacitance was found by plotting the right side of equation vs. the range of scan rate. The ECSA subsequently identified as the difference between the capacitance of the PTFE GDEs compared to a flat 1 cm^2 Cu surface[25].

RESULTS

Modification of Cu nanoparticles surface with imidazolium-based ionic liquids

A gas diffusion electrode (GDE) was prepared via deposition of Cu nanoparticles (CuNPs) on a polytetrafluoroethylene (PTFE) membrane. The resulting GDE was implemented into a gas-fed flow cell (Figure 1a), activated (see experimental section) and proved to be catalytically active for the electroreduction of an aqueous solution of 1-ethyl-3-methylimidazolium tetrafluoroborate ($EMIMBF_4$), as shown from the in-situ Linear Sweep Voltammogram (LSV) in Figure 1b, with a catalytic wave appearing at a more cathodic potential than -1.4 V vs. Ag/AgCl. During reduction, an EMIM-derived organic layer deposited on the surface of the electrode, as discussed below. As a consequence, modification of the Cu material surface was achieved by electrodeposition of $EMIMBF_4$ following a methodology described in the experimental section.

Optimization of the $EMIMBF_4$ deposition process was carried out under inert atmosphere by varying the applied cathodic current density (-10 to -50 $mA.cm^{-2}$ during 10 min) and the time of deposition (5-60 min

at -10 mA.cm^{-2}) and testing each electrode for selective CO_2 electroreduction to multicarbon (C_{2+}) products at -200 mA.cm^{-2} during 30 minutes. In this case, the anode of the flow cell was a Ni foam and CO_2 was supplied as a gas at the backside of the gas diffusion cathode, with a flow rate of 10 mL.min^{-1}. More specifically, the flowing catholyte, 0.05 M H_2SO_4 + 3M KCl, was acidic (pH = 0.89), the flowing anolyte, 2.5 M KOH, was alkaline in order to allow the utilization of non-noble metals at the anode[16]. The two compartments were separated by a bipolar membrane, which maintains the pH gradient, thanks to the water dissociation reaction occurring at the interlayer, and prevents crossover of cationic electrolyte species[43–46].

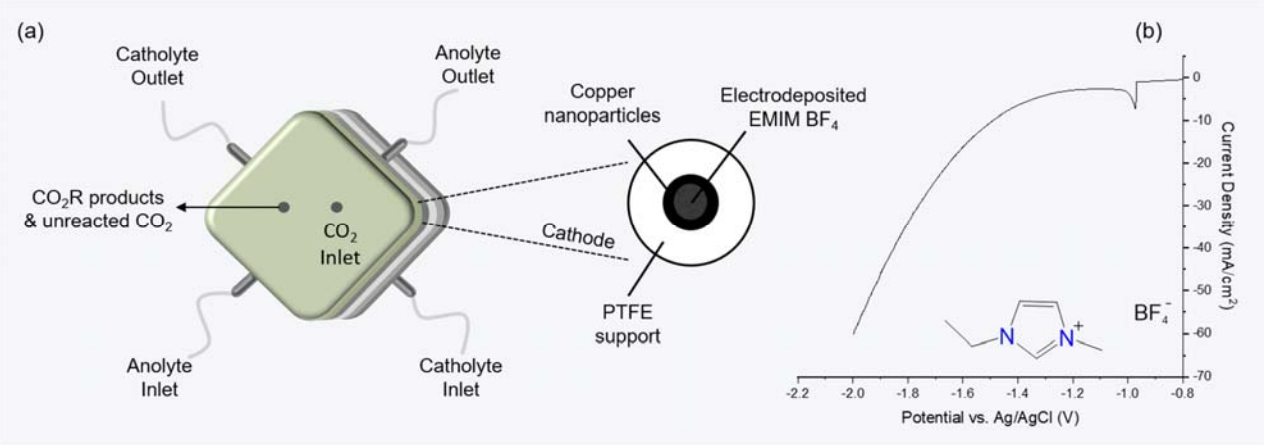

Figure 1. (a) Schematic representation of the flow-cell setup used and (b) LSV of 0.5 M EMIMBF$_4$ aqueous solution within the flow-cell setup using a CuNP GDE cathode. Scan rate (25 mV.s^{-1}).

The results of the optimization process are displayed in Figure S2. They clearly show the following trends: (i) low faradic Efficiency for H_2 (FE_{H2} < 10 %) were obtained, in spite of the very acidic conditions, except when deposition was carried out at the highest cathodic current density (-50 mA.cm^{-2}) and when long deposition times are used (60 min); (ii) modification of the surface of CuNPs favored C_{2+} products formation, the highest effect being observed for an applied current density of -10 mA.cm^{-2} and a deposition time of 30 minutes. In the following only this electrode, named CuNP-EMIM, will be discussed.

CO_2 electroreduction under acidic conditions

The effect of the modification of the electrode was tested by CO_2 electrolysis at various applied current densities (-50 to -300 mA.cm^{-2}). The results are shown in Figure 2 and Figure S3 where FE values of the reaction products are reported either combined as C_1 and C_{2+} products or individually, respectively. As

shown in Figure 2, the CuNP-EMIM electrode proved indeed much more selective for C_{2+} than for C_1 products, especially at high current densities (Figure 2b). While the unmodified electrode produced more C_1 than C_{2+} products at all tested current densities (Figure 2a), a much larger decrease of C_1 products and larger increase of C_{2+} products were observed using the CuNP-EMIM electrode upon increasing the current density as compared to the unmodified electrode. As a matter of fact, the C_{2+}/C_1 ratio was higher in the case of the CuNP-EMIM electrode at all applied current densities and reached a remarkable value of 4 at -300 mA.cm^{-2} (Figure 2c).

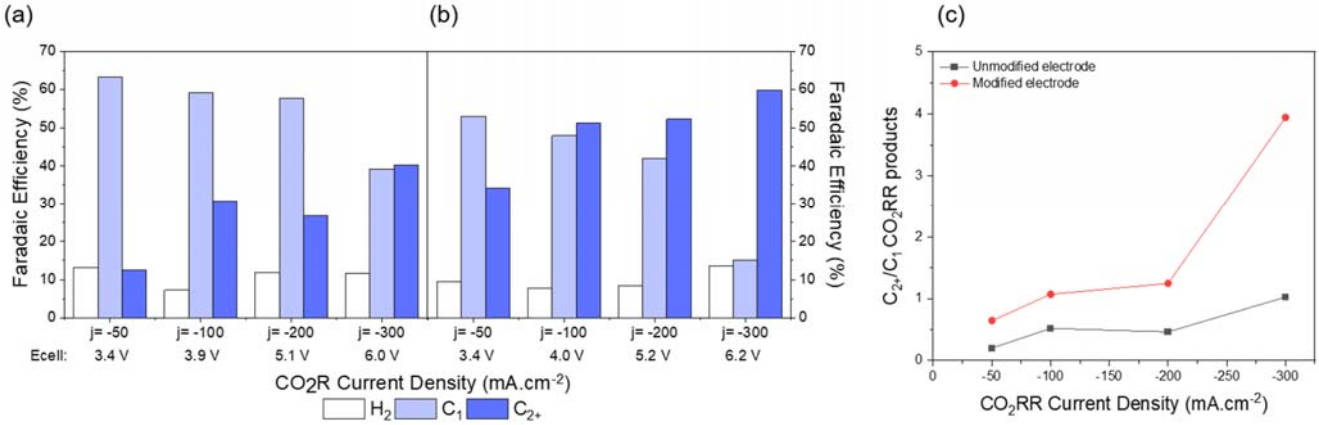

Figure 2. (a,b) Faradic Efficiency for H_2, C_1 and C_{2+} products formation using: (a) the unmodified electrode or (b) the CuNP-EMIM electrode and (c) C_{2+}/C_1 ratio as a function of applied current density. CO_2RR performed in an acidic catholyte (0.05 M H_2SO_4 + 3 M KCl, pH = 0.89) under a CO_2 flow of 10 mL.min^{-1} at different current densities for 30 minutes each.

Long term electrolysis was carried out with an applied current density of -200 mA.cm^{-2} using both unmodified and modified Cu electrodes. The results are shown in Figure 3. First, we note that the working electrode potential and the Faradic Efficiencies for all products were remarkably stable during 5 hours, indicating no or limited loss of the imidazolium-based layer during electrolysis. As expected, faradic efficiencies for ethanol, propanol and ethylene were much larger in the case of the CuNP-EMIM modified electrode (Figure 3a) while the faradic efficiencies for CO and formic acid were much greater in the case of the unmodified electrode (Figure 3b). Thus, modification of commercial CuNPs with $EMIMBF_4$ provides a stable material with increased selectivity for C_{2+} products. Comparison of Figure 3a and 3b shows an increase by approximately a factor of 2 for the production of ethylene (FE = 22 %), ethanol (FE = 14 %) and propanol (FE = 9.5 %), while acetic acid remained unchanged. It is thus remarkable that at a high current

density of -200 mA.cm^{-2}, under acidic conditions, the modified catalyst allowed a total Faradic efficiency for C_{2+} products of 47 % (as compared to 27 % for the unmodified one).

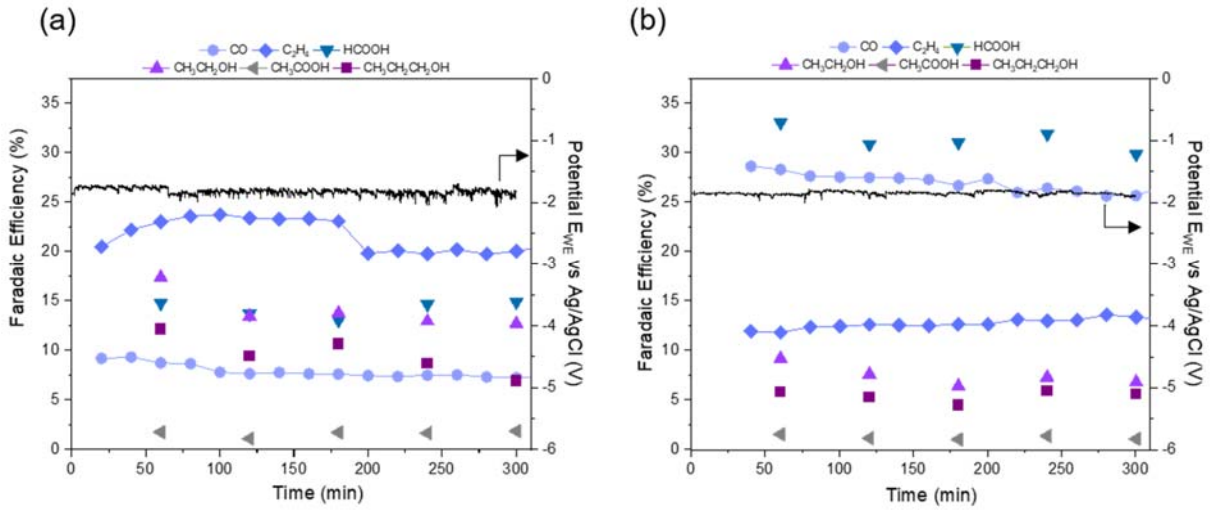

Figure 3. Evolution of CO_2RR product distribution and working electrode potential during CO_2 electroreduction using (a) the CuNP-EMIM electrode and (b) the unmodified electrode. CO_2RR performed in an acidic catholyte (0.05 M H_2SO_4 + 3 M KCl, pH = 0.89) under a CO_2 flow of 10 mL.min^{-1} at -200 mA.cm^{-2} during 5 hours.

In order to show that this effect was not specific for the selected CuNPs, we have carried out the same study with another source of Cu material. For this study we have used Cu NPs, named STCu200, that were obtained by a simple solvothermal procedure, using a solution of Cu(acetate)$_2$ in ethanol which was heated to 200 °C in an autoclave for 20 h (see experimental section). After electrodeposition of $EMIMBF_4$ (for 10 min with an applied current density of -10 mA.cm^{-2}), the modified STCu200 was used for CO_2 electroreduction at -200 mA.cm^{-2}. The results in Figure S4 clearly showed a larger C_{2+}/C_1 ratio as compared to the unmodified electrode (from 0.6 to 2), with approximately no change in the Faradic Efficiency for H_2.

Characterization of the layer deposited on CuNP-EMIM electrode

Scanning Electron Microscopy (SEM) images of the modified electrode clearly showed the presence of a thin organic layer on the surface on the Cu NPs (Figures 4a and S4), with CuNPs and the layer having together a total thickness of approximatively 8 µm. Energy Dispersive X-ray (EDX) spectroscopy confirmed the presence of N, B and F signals likely derived from $EMIMBF_4$ (Figures 4b and S5). SEM and EDX also

showed that these features were retained after acidic electrolysis (Figure S54 and S6). Elemental mapping showed that N, B and F were all homogeneously dispersed on the CuNPs surface, all arising from the IL used ($EMIMBF_4$) (Figures 4c and S7). We also observed the presence of some isolated crystals on the electrode surface, containing potassium, likely leftover from the electrode initial activation step. Furthermore, X-ray Photoelectron Spectrometry (XPS) analysis further proved the presence of N, which can only be derived from $EMIMBF_4$ on the surface both after deposition and after subsequent acidic electrolysis (Figures 4d and S8). From the deconvolution of the N 1s XPS spectrum of the CuNP-EMIM electrode (Figure 4d and S8), three peaks, at a binding energy of 398.9 eV (green), 400.5 eV (blue) and 401.7 eV (red), were observed, in agreement with previously reported XPS data for imidazolium species immobilized on metallic surfaces [39,47–49]. The analysis of the N signals in the EDX and XPS spectra though indicated a small decrease in their intensity following electrolysis, suggesting a minor loss of the layer during electrolysis, however with no major impact on the selectivity (see Figure 3). The Cu 2p XPS spectrum was not affected by the presence of the layer, as shown from the comparison between spectra of CuNPs and CuNP-EMIM after electrolysis (Figure S8). The ATR-FTIR spectrum (Figure 4e and f) of the CuNP-EMIM electrode (blue plot) displayed bands, absent from the spectrum of the unmodified electrode (black plot), that, by comparison with the spectrum of pure $EMIMBF_4$ (red plot), confirmed the presence of an EMIM-like structure on the surface: a band at 1165 cm^{-1} characteristic of methyl-N and ethyl-N stretching, a band at 1564 cm^{-1}, corresponding to C=C stretching and the bands at 3118 and 3158 cm^{-1}, reflecting C_2-H stretching and C_4-H, C_5-H stretching of the imidazolium ring, respectively[50,51]. The band at 1010 cm^{-1} is associated with the counter anion of the IL used for electrodeposition. Finally, modification of the surface was consistent with the observed variation of the water contact angle (WCA). Figure S9 shows that WCA diminished from 156° in the unmodified electrode to 107° in the CuNP-EMIM electrode, reflecting a slightly more hydrophilic surface and that WCA increased only a little bit after electrolysis.

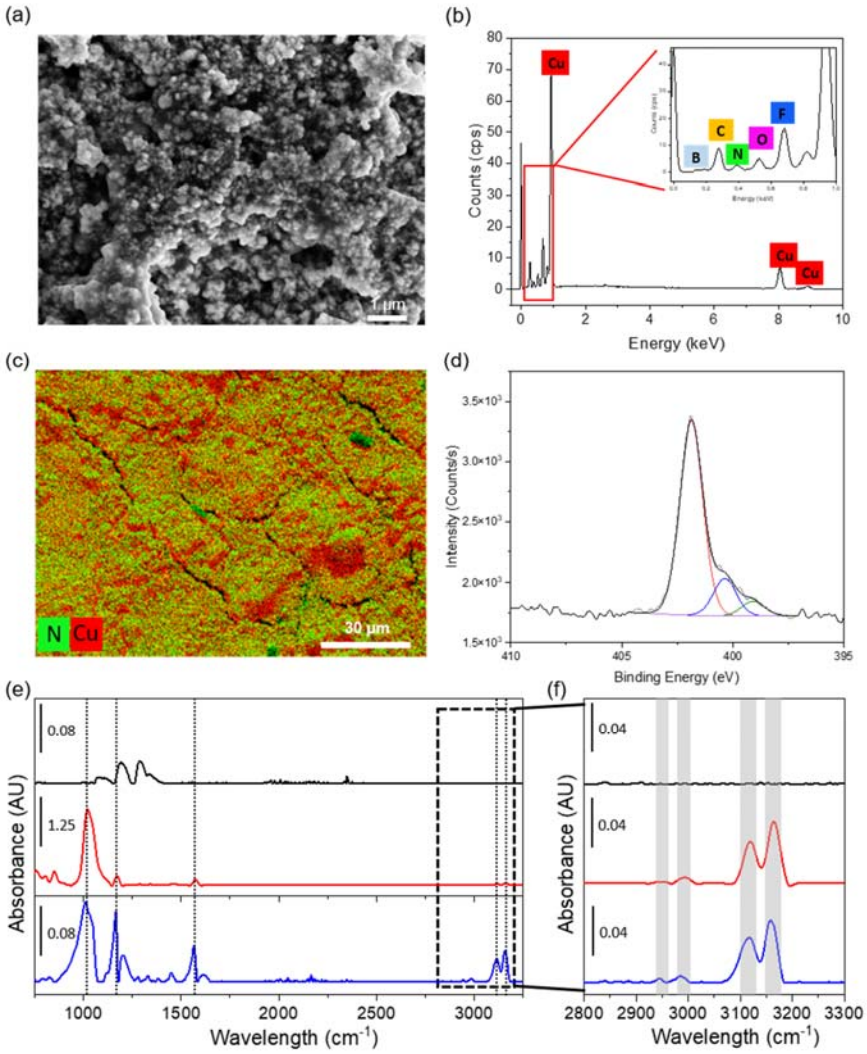

Figure 4. Characterization of the CuNP-EMIM electrode by (a) SEM image, (b) EDX analysis with inlet zoom on the zone from 0 to 1 keV, (c) EDX elemental mapping superposing N (green) and Cu (red), (d) N 1s XPS spectrum and (e) ATR-FTIR (blue plot), where (f) is a zoom of the 3000 cm^{-1} regions compared to an unmodified electrode (black plot) and a drop of pure $EMIMBF_4$ (red plot).

Electrochemical surface area (ECSA) of the different electrodes were determined via measurement of double layer capacitances (Figure S10 and Table S1). They showed that electrodeposition of the imidazolium-based layer had no effect on the roughness of the electrode surface since the ECSA values were the same (at about 55 $cm^2.cm^{-2}$) whether the CuNPs had undergone modification or not and similarly no significant ECSA change could be observed after electrolysis.

EMIM-derived layer allows potassium-free CO_2RR and partially prevents HER.

As well established, alkali metal cations, and particularly K^+ cations, are critical components of the electrolyte for acidic CO_2 electrolysis, as they contribute to HER suppression[18,19]. This is what we clearly show in Figure 5 using the unmodified electrode. In the absence of KCl in a highly acidic solution (0.1 M H_2SO_4, pH = 0.7), an unmodified Cu NP electrode produced exclusively H_2 at -100 mA.cm^{-2}, as can be observed from Faradaic Efficiency values of cumulative CO_2RR products and H_2. The HER inhibitory effect of K^+ cations was clear from the decrease of FE_{H2} and the increase of FE for CO_2 products upon increasing the concentration of K^+ in the electrolyte (Figure 5a) by reaching a maximum FE ≈ 60 % for CO_2 products in the presence of 3 M KCl. Interestingly, in contrast with the unmodified electrode, CO_2 products were observed using the CuNP-EMIM electrode, in the absence of KCl in the solution (Figure 5b). The FE for CO_2 products was 11 %, indicating a significant HER suppressing effect of the EMIM-based layer comparable to that of a KCl concentration of approximatively 0.8 M in the acidic catholyte. Furthermore, if the electrodeposition was performed in three consecutive steps of 10 minutes at -10 mA/cm^2 each, the resulting FE for CO_2 products increased to 15 %. This effect is consistent with the positive charge of the immobilized EMIM-based material on Cu NPs, which limits H^+ reduction and H_2 evolution. While limited, the effect observed here illustrates for the first time a possible strategy for circumventing the need for a large concentration of M^+ ions in order to inhibit HER in acidic electrolytes. Following this proof-of-concept, further studies will aim at finding more efficient Cu surface modifiers in that respect.

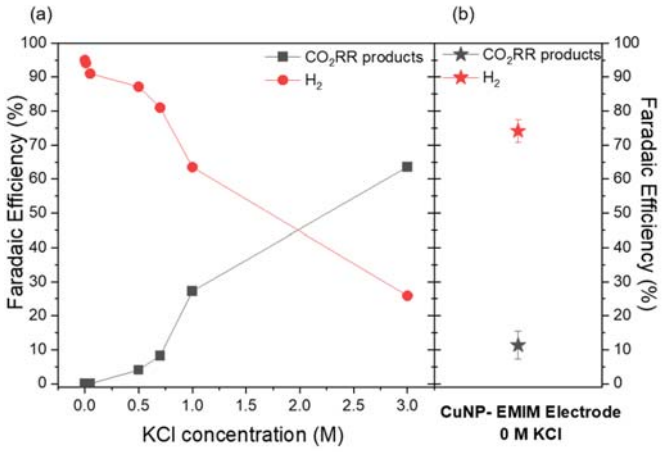

Figure 5. Faradaic Efficiencies of H_2 and CO_2RR product distribution during CO_2 electroreduction using: (a) an unmodified electrode in a 0.1 M H_2SO_4 solution with increasing KCl concentrations and (b) the CuNP-EMIM electrode in a 0.1 M H_2SO_4 solution without KCl. CO_2RR performed at -100 mA.cm^{-2} under a CO_2 flow of 10 mL.min^{-1} for 30 minutes each.

CONCLUSION

So far, only few studies have explored the potential of Cu materials as catalysts for CO_2 electroreduction under acidic conditions at industrially relevant current densities[15–17,19]. As under neutral and alkaline conditions, Cu has the advantage of allowing C-C coupling generating C_{2+} products, and its ability to form multicarbon products is not altered even in highly acidic electrolytes. However, it remains poorly selective, generating H_2, a mixture of C_1 products, notably CO and HCOOH, and a complex mixture of C_{2+} product such as ethylene, ethanol, acetic acid and propanol. Acidic CO_2 electrolysis thus calls for strategies aiming at tuning the selectivity of Cu-based electrocatalytic materials. Here, we show a rather drastic change of selectivity, both in terms of CO_2RR vs HER and C_{2+} vs C_1 using Cu NPs surface molecular modification, opening a new direction towards the discovery of selective Cu-based catalysts. Such a strategy has been already used for standard neutral or alkaline CO_2 electrolysis, but not for acidic electrolysis under industrially relevant current densities[23]. During the course of this work, another study was published, showing a comparable effect with Cu electrodes modified with pyridinium[26]. This was achieved here thanks to an easy electrodeposition of a stable imidazolium-based layer on the surface of CuNPs, which was shown to inhibit HER and C_1 products formation and favor instead ethylene and ethanol formation. While a positive charge on the surface, actually mimicking a K^+ layer, may explain the HER inhibition effect, the mechanism by which the organic layer favors C-C coupling is less clear at present. It is very likely, as previously proposed, that it contributes to the stabilization of adsorbed intermediate *CO, thus favoring C-C coupling, and of adsorbed C_{2+} intermediates[26,39]. Interestingly, the EMIM-based layer can exert its effect also in the absence of K^+ ions, supporting the concept of using positively charged species on Cu surface as substitutes for alkali cations. This work thus contributes to addressing optimization of the conditions needed for selective CO_2 electroreduction at acidic pH (< 1) and calls for further investigations with various families of molecular modifiers.

ACKNOWLEDGEMENTS

This work was supported financially by funding from Total Research & Technology Feluy. We thank Françoise Pillier (Laboratoire Interfaces et Systèmes Electrochimiques, UMR 8235) for SEM and EDX analysis and Antoine Miche (Laboratoire de Réactivité de Surface, UMR 7197) for XPS characterization. The authors acknowledge the support of the Centre National de la Recherche Scientifique (CNRS).

ASSOCIATED CONTENT

Supporting Information. See Supporting Information for full faradaic efficiency profiles, detailed characterization of electrodes, and ECSA measurements. This material is available free of charge via the Internet at http://pubs.acs.org.

AUTHOR INFORMATION

Corresponding Authors * Email: marc.fontecave@college-de-france.fr; carlos.sanchez@sorbonne-universite.fr; maria.gomez@college-de-france.fr.

ORCID

Alessandro Perazio: 0000-0001-8204-4362

Maria Gomez Mingot: 0000-0002-1557-2648

Carlos M. Sánchez-Sánchez: 0000-0003-4285-4648

Marc Fontecave: 0000-0002-8016-4747

REFERENCES

(1) Nitopi, S.; Bertheussen, E.; Scott, S. B.; Liu, X.; Engstfeld, A. K.; Horch, S.; Seger, B.; Stephens, I. E. L.; Chan, K.; Hahn, C.; *et al*. Progress and Perspectives of Electrochemical CO_2 Reduction on Copper in Aqueous Electrolyte. *Chem. Rev.* **2019**, *119*, 7610–7672.

(2) Zhao, J.; Xue, S.; Barber, J.; Zhou, Y.; Meng, J.; Ke, X. An Overview of Cu-Based Heterogeneous Electrocatalysts for CO_2 Reduction. *J. Mater. Chem. A* **2020**, *8*, 4700–4734.

(3) Creissen, C. E.; Fontecave, M. Solar-Driven Electrochemical CO_2 Reduction with Heterogeneous Catalysts. *Adv. Energy Mater.* **2021**, *11*, 2002652.

(4) Karapinar, D.; Creissen, C. E.; Rivera de la Cruz, J. G.; Schreiber, M. W.; Fontecave, M. Electrochemical CO_2 Reduction to Ethanol with Copper-Based Catalysts. *ACS Energy Lett.* **2021**, *6*, 694–706.

(5) Todorova, T. K.; Schreiber, M. W.; Fontecave, M. Mechanistic Understanding of CO_2 Reduction Reaction (CO_2RR) Toward Multicarbon Products by Heterogeneous Copper-Based Catalysts. *ACS Catal.* **2020**, *10*, 1754–1768.

(6) Li, F.; Thevenon, A.; Rosas-Hernández, A.; Wang, Z.; Li, Y.; Gabardo, C. M.; Ozden, A.; Dinh, C. T.; Li, J.; Wang, Y.; *et al.* Molecular Tuning of CO_2-to-Ethylene Conversion. *Nature* **2020**, *577*, 509–513.

(7) Chen, X.; Chen, J.; Alghoraibi, N. M.; Henckel, D. A.; Zhang, R.; Nwabara, U. O.; Madsen, K. E.; Kenis, P. J. A.; Zimmerman, S. C.; Gewirth, A. A. Electrochemical CO_2-to-Ethylene Conversion on Polyamine-Incorporated Cu Electrodes. *Nat. Catal.* **2021**, *4*, 20–27.

(8) Hori, Y. Electrochemical CO_2 Reduction on Metal Electrodes. In *Modern Aspects of Electrochemistry*; Vayenas, C. G., White, R. E., Gamboa-Aldeco, M. E., Eds.; Modern Aspects of Electrochemistry; Springer: New York, NY, 2008.

(9) Zhao, S.; Christensen, O.; Sun, Z.; Liang, H.; Bagger, A.; Torbensen, K.; Nazari, P.; Lauritsen, J. V.; Pedersen, S. U.; Rossmeisl, J.; *et al.* Steering Carbon Dioxide Reduction toward C–C Coupling Using Copper Electrodes Modified with Porous Molecular Films. *Nat. Commun.* **2023**, *14*, 844.

(10) Zhang, L.; Merino-Garcia, I.; Albo, J.; Sánchez-Sánchez, C. M. Electrochemical CO_2 Reduction Reaction on Cost-Effective Oxide-Derived Copper and Transition Metal–Nitrogen–Carbon Catalysts. *Curr. Opin. Electrochem.* **2020**, *23*, 65–73.

(11) Ma, D.; Jin, T.; Xie, K.; Huang, H. An Overview of Flow Cell Architecture Design and Optimization for Electrochemical CO_2 Reduction. *J. Mater. Chem. A* **2021**, *9*, 20897–20918.

(12) Wakerley, D.; Lamaison, S.; Wicks, J.; Clemens, A.; Feaster, J.; Corral, D.; Jaffer, S. A.; Sarkar, A.; Fontecave, M.; Duoss, E. B.; *et al*. Gas Diffusion Electrodes, Reactor Designs and Key Metrics of Low-Temperature CO_2 Electrolysers. *Nat. Energy* **2022**, *7*, 130–143.

(13) Rabinowitz, J. A.; Kanan, M. W. The Future of Low-Temperature Carbon Dioxide Electrolysis Depends on Solving One Basic Problem. *Nat. Commun.* **2020**, *11*, 5231.

(14) Chen, C.; Li, Y.; Yang, P. Address the "Alkalinity Problem" in CO_2 Electrolysis with Catalyst Design and Translation. *Joule* **2021**, *5*, 737–742.

(15) Hao, Q.; Liu, D.-X.; Zhong, H.-X.; Tang, Q.; Yan, J.-M. Electrocatalytic CO_2 Reduction in Acidic Medium. *Chem Catal.* **2023**, *3*, 100542.

(16) Huang, J. E.; Li, F.; Ozden, A.; Sedighian Rasouli, A.; García de Arquer, F. P.; Liu, S.; Zhang, S.; Luo, M.; Wang, X.; Lum, Y.; *et al.* CO_2 Electrolysis to Multicarbon Products in Strong Acid. *Science* **2021**, *372*, 1074–1078.

(17) Ma, Z.; Yang, Z.; Lai, W.; Wang, Q.; Qiao, Y.; Tao, H.; Lian, C.; Liu, M.; Ma, C.; Pan, A.; *et al.* CO_2 Electroreduction to Multicarbon Products in Strongly Acidic Electrolyte via Synergistically Modulating the Local Microenvironment. *Nat. Commun.* **2022**, *13*, 7596.

(18) Monteiro, M. C. O.; Dattila, F.; Hagedoorn, B.; García-Muelas, R.; López, N.; Koper, M. T. M. Absence of CO_2 Electroreduction on Copper, Gold and Silver Electrodes without Metal Cations in Solution. *Nat. Catal.* **2021**, *4*, 654–662.

(19) Gu, J.; Liu, S.; Ni, W.; Ren, W.; Haussener, S.; Hu, X. Modulating Electric Field Distribution by Alkali Cations for CO_2 Electroreduction in Strongly Acidic Medium. *Nat. Catal.* **2022**, *5*, 268–276.

(20) Qin, H.-G.; Li, F.-Z.; Du, Y.-F.; Yang, L.-F.; Wang, H.; Bai, Y.-Y.; Lin, M.; Gu, J. Quantitative Understanding of Cation Effects on the Electrochemical Reduction of CO_2 and H^+ in Acidic Solution. *ACS Catal.* **2023**, *13*, 916–926.

(21) Ma, Y.; Wang, J.; Yu, J.; Zhou, J.; Zhou, X.; Li, H.; He, Z.; Long, H.; Wang, Y.; Lu, P.; *et al.* Surface Modification of Metal Materials for High-Performance Electrocatalytic Carbon Dioxide Reduction. *Matter* **2021**, *4*, 888–926.

(22) Zhu, Q.; Murphy, C. J.; Baker, L. R. Opportunities for Electrocatalytic CO_2 Reduction Enabled by Surface Ligands. *J. Am. Chem. Soc.* **2022**, *144*, 2829–2840.

(23) Christensen, O.; Zhao, S.; Sun, Z.; Bagger, A.; Lauritsen, J. V.; Pedersen, S. U.; Daasbjerg, K.; Rossmeisl, J. Can the CO_2 Reduction Reaction Be Improved on Cu: Selectivity and Intrinsic Activity of Functionalized Cu Surfaces. *ACS Catal.* **2022**, *12*, 15737–15749.

(24) Creissen, C. E.; Rivera de la Cruz, J. G.; Karapinar, D.; Taverna, D.; Schreiber, M. W.; Fontecave, M. Molecular Inhibition for Selective CO_2 Conversion. *Angew. Chem. Int. Ed.* **2022**, *61*, e202206279.

(25) Wakerley, D.; Lamaison, S.; Ozanam, F.; Menguy, N.; Mercier, D.; Marcus, P.; Fontecave, M.; Mougel, V. Bio-Inspired Hydrophobicity Promotes CO_2 Reduction on a Cu Surface. *Nat. Mater.* **2019**, *18*, 1222–1227.

(26) Nie, W.; Heim, G. P.; Watkins, N. B.; Agapie, T.; Peters, J. C. Organic Additive-Derived Films on Cu Electrodes Promote Electrochemical CO_2 Reduction to C_{2+} Products Under Strongly Acidic Conditions. *Angew. Chem. Int. Ed Engl.* **2023**, *62*, e202216102.

(27) Vichou, E.; Li, Y.; Gomez-Mingot, M.; Fontecave, M.; Sánchez-Sánchez, C. M. Imidazolium- and Pyrrolidinium-Based Ionic Liquids as Cocatalysts for CO_2 Electroreduction in Model Molecular Electrocatalysis. *J. Phys. Chem. C* **2020**, *124*, 23764–23772.

(28) Vichou, E.; Solé-Daura, A.; Mellot-Draznieks, C.; Li, Y.; Gomez-Mingot, M.; Fontecave, M.; Sánchez-Sánchez, C. M. Electrocatalytic Conversion of CO_2 to Formate at Low Overpotential by Electrolyte Engineering in Model Molecular Catalysis. *ChemSusChem* **2022**, *15*, e202201566.

(29) Sánchez-Sánchez, C. M. Electrocatalytic Reduction of CO_2 in Imidazolium-Based Ionic Liquids. In *Reference Module in Chemistry, Molecular Sciences and Chemical Engineering. Encyclopedia of Interfacial Chemistry: Surface Science and Electrochemistry*; Wandelt, K., Ed.; Elsevier, 2018.

(30) Hanc-Scherer, F. A.; Montiel, M. A.; Montiel, V.; Herrero, E.; Sánchez-Sánchez, C. M. Surface Structured Platinum Electrodes for the Electrochemical Reduction of Carbon Dioxide in Imidazolium Based Ionic Liquids. *Phys. Chem. Chem. Phys.* **2015**, *17*, 23909–23916.

(31) Rosen, B. A.; Salehi-Khojin, A.; Thorson, M. R.; Zhu, W.; Whipple, D. T.; Kenis, P. J. A.; Masel, R. I. Ionic Liquid–Mediated Selective Conversion of CO_2 to CO at Low Overpotentials. *Science* **2011**, *334*, 643–644.

(32) Lau, G. P. S.; Schreier, M.; Vasilyev, D.; Scopelliti, R.; Grätzel, M.; Dyson, P. J. New Insights Into the Role of Imidazolium-Based Promoters for the Electroreduction of CO_2 on a Silver Electrode. *J. Am. Chem. Soc.* **2016**, *138*, 7820–7823.

(33) Zhao, S.-F.; Horne, M.; Bond, A. M.; Zhang, J. Is the Imidazolium Cation a Unique Promoter for Electrocatalytic Reduction of Carbon Dioxide? *J. Phys. Chem. C* **2016**, *120*, 23989–24001.

(34) Koshy, D. M.; Akhade, S. A.; Shugar, A.; Abiose, K.; Shi, J.; Liang, S.; Oakdale, J. S.; Weitzner, S. E.; Varley, J. B.; Duoss, E. B.; *et al.* Chemical Modifications of Ag Catalyst Surfaces with Imidazolium Ionomers Modulate H_2 Evolution Rates during Electrochemical CO_2 Reduction. *J. Am. Chem. Soc.* **2021**, *143*, 14712–14725.

(35) Parada, W. A.; Vasilyev, D. V.; Mayrhofer, K. J. J.; Katsounaros, I. CO_2 Electroreduction on Silver Foams Modified by Ionic Liquids with Different Cation Side Chain Length. *ACS Appl. Mater. Interfaces* **2022**, *14*, 14193–14201.

(36) Iijima, G.; Kitagawa, T.; Katayama, A.; Inomata, T.; Yamaguchi, H.; Suzuki, K.; Hirata, K.; Hijikata, Y.; Ito, M.; Masuda, H. CO_2 Reduction Promoted by Imidazole Supported on a Phosphonium-Type Ionic-Liquid-Modified Au Electrode at a Low Overpotential. *ACS Catal.* **2018**, *8*, 1990–2000.

(37) Neyrizi, S.; Kiewiet, J.; Hempenius, M. A.; Mul, G. What It Takes for Imidazolium Cations to Promote Electrochemical Reduction of CO_2. *ACS Energy Lett.* **2022**, *7*, 3439–3446.

(38) Cheng, B.; Du, J.; Yuan, H.; Tao, Y.; Chen, Y.; Lei, J.; Han, Z. Selective CO_2 Reduction to Ethylene Using Imidazolium-Functionalized Copper. *ACS Appl. Mater. Interfaces* **2022**, *14*, 27823–27832.

(39) Sha, Y.; Zhang, J.; Cheng, X.; Xu, M.; Su, Z.; Wang, Y.; Hu, J.; Han, B.; Zheng, L. Anchoring Ionic Liquid in Copper Electrocatalyst for Improving CO_2 Conversion to Ethylene. *Angew. Chem. Int. Ed.* **2022**, *61*, e202200039.

(40) Li, X.-Q.; Duan, G.-Y.; Chen, J.-W.; Han, L.-J.; Zhang, S.-J.; Xu, B.-H. Regulating Electrochemical CO_2RR Selectivity at Industrial Current Densities by Structuring Copper@poly(Ionic Liquid) Interface. *Appl. Catal. B Environ.* **2021**, *297*, 120471.

(41) Duan, G.-Y.; Li, X.-Q.; Ding, G.-R.; Han, L.-J.; Xu, B.-H.; Zhang, S.-J. Highly Efficient Electrocatalytic CO2 Reduction to C_{2+} Products on a Poly(Ionic Liquid)-Based Cu^0–Cu^I Tandem Catalyst. *Angew. Chem. Int. Ed.* **2022**, *61*, e202110657.

(42) Hong, Z-S.; Cao, Y.; Deng, J-F. A Convenient Alcohothermal Approach for Low Temperature Synthesis of CuO Nanoparticles. *Mater. Lett.* **2002**, *52*, 34–38.

(43) Ma, M.; Kim, S.; Chorkendorff, I.; Seger, B. Role of Ion-Selective Membranes in the Carbon Balance for CO_2 Electroreduction via Gas Diffusion Electrode Reactor Designs. *Chem. Sci.* **2020**, *11*, 8854–8861.

(44) Peugeot, A.; Creissen, C. E.; Schreiber, M. W.; Fontecave, M. Advancing the Anode Compartment for Energy Efficient CO_2 Reduction at Neutral PH. *ChemElectroChem* **2021**, *8*, 2726–2736.

(45) Yan, Z.; Hitt, J. L.; Zeng, Z.; Hickner, M. A.; Mallouk, T. E. Improving the Efficiency of CO_2 Electrolysis by Using a Bipolar Membrane with a Weak-Acid Cation Exchange Layer. *Nat. Chem.* **2021**, *13*, 33–40.

(46) Xie, K.; Miao, R. K.; Ozden, A.; Liu, S.; Chen, Z.; Dinh, C.-T.; Huang, J. E.; Xu, Q.; Gabardo, C. M.; Lee, G.; *et al.* Bipolar Membrane Electrolyzers Enable High Single-Pass CO_2 Electroreduction to Multicarbon Products. *Nat. Commun.* **2022**, *13*, 3609.

(47) Villar-Garcia, I. J.; Smith, E. F.; Taylor, A. W.; Qiu, F.; Lovelock, K. R. J.; Jones, R. G.; Licence, P. Charging of Ionic Liquid Surfaces under X-Ray Irradiation: The Measurement of Absolute Binding Energies by XPS. *Phys Chem Chem Phys* **2011**, *13*, 2797–2808.

(48) Men, S.; Mitchell, D. S.; Lovelock, K. R. J.; Licence, P. X-Ray Photoelectron Spectroscopy of Pyridinium-Based Ionic Liquids: Comparison to Imidazolium- and Pyrrolidinium-Based Analogues. *ChemPhysChem* **2015**, *16*, 2211–2218.

(49) Chi, Y. S.; Hwang, S.; Lee, B. S.; Kwak, J.; Choi, I. S.; Lee, S. Anion Exchange-Promoted $Ru^{3+/2+}$ Redox Switch in Self-Assembled Monolayers of Imidazolium Ions on a Gold Electrode. *Langmuir* **2005**, *21*, 4268–4271.

(50) Katsyuba, S. A.; Dyson, P. J.; Vandyukova, E. E.; Chernova, A. V.; Vidiš, A. Molecular Structure, Vibrational Spectra, and Hydrogen Bonding of the Ionic Liquid 1-Ethyl-3-Methyl-1H-Imidazolium Tetrafluoroborate. *Helv. Chim. Acta* **2004**, *87*, 2556–2565.

(51) Papasizza, M.; Cuesta, A. In Situ Monitoring Using ATR-SEIRAS of the Electrocatalytic Reduction of CO_2 on Au in an Ionic Liquid/Water Mixture. *ACS Catal.* **2018**, *8*, 6345–6352.

TABLE OF CONTENTS (TOC) GRAPHIC